Journal of Marine Science and Engineering

MDPI

Article

Response of Sedimentary Dynamics to Tropical Cyclones under Various Scenarios in Jiangsu Coast

Can Wang [a], Chengyi Zhao [a]*, Gang Yang [b], Chunhui Li [b], Jianting Zhu [c] and Xiaofei Ma [a]

[a] School of Geographical Sciences, Nanjing University of Information Science and Technology, Nanjing 210044, China.
[b] School of Marine Sciences, Nanjing University of Information Science and Technology, Nanjing 210044, China.
[c] Department of Civil and Architectural Engineering, University of Wyoming, Laramie, WY 82071, USA.
* Correspondence: Chengyi (C.Y.) Zhao, School of Geographic Sciences, Nanjing University of Information Sciences and Technology, No.219 Ningliu Road, Nanjing, 210044, China; Telephone/Fax: +86-25-58235199; Email address: zhaocy@nuist.edu.cn

Abstract: Jiangsu Coast (JC), China is a tropical cyclone (TC) highly impact area. However, due to the lack of available on-site observation data, nearshore sedimentary dynamic processes under the impact of TCs have been little explored. This study developed a 3D wave-current-sediment numerical model for JC based on the Finite Volume Coastal Ocean Model (FVCOM) to investigate sediment dynamic response to TCs in various scenarios. The results indicated that typhoons can significantly impact the hydrodynamics and sediment dynamics of JC. During Typhoon Lekima in 2019, strong southeasterly winds led to a substantial increase in current velocity, bottom stress, wave height, and SSC. Three typical landfall-type typhoons, with prevailing southeasterly winds, brought significant sediment flux from southeast to northwest along the coast, while the typhoon moved northward in the Yellow Sea bringing a relatively smaller sediment flux from north to south. Typhoons can also induce stripe-like erosion and deposition which is closely related to seafloor topography, resulting in seabed thickness variations of up to ±0.3m. Additionally, strengthening typhoon wind fields can lead to increased sediment flux and seabed morphological changes. Typhoon 9711, particularly at spring tide, had a greater impact on sediment dynamics compared to other landfall typhoons. Numerical simulations showed that the typhoon-induced net sediment flux within the spring tidal cycle could increase by 80% to 100% compared to the neap tidal cycle, indicating the significant influence of tidal conditions on sediment transport during TC events.

Keywords: Jiangsu Coast; Numerical modeling; Tropical cyclone; Sedimentary dynamic processes; Morphological change

1. Introduction

Tropical cyclones (TCs) are disastrous weather systems, often accompanied by gales, rainstorms, huge waves, and storm surges [1]. The strong interaction between the atmosphere and the ocean can significantly affect coastal hydrodynamics, and the seabed morphology may undergo certain changes after a series of processes such as sediment resuspension, transport, and sedimentation [2]. In some cases, TC events may contribute nearly half of the seasonal net sediment transport [3], even two orders of magnitude more than sediment transport under fair weather conditions [4,5]. Theoretical and modeling results indicate that future global warming may lead to an increasing potential for tropical cyclone destruction, which may threaten the safety of residents' lives and property in coastal areas [6]. Therefore, it is essential to enhance our comprehension of sediment dynamics under TC effects to provide a theoretical basis for coastal management and disaster prevention and mitigation.

According to on-site observations, both Typhoons No. 8114 and No. 9711 significantly increased the water level and wave height along the eastern coast of China, causing significant changes in the morphology of tidal flats [7,8]. Yang, *et al.* [1] found that the strong wave current interaction caused by Typhoon No. 1909 greatly increased bottom stress which affected sediment transport. Zhang, *et al.* [9] found that typhoons directly landing along the coast of Jiangsu can increase storm surge in the radial sand ridge (RSR) area by up to nearly 3 meters. Based on the study of Cong, *et al.* [10], the waves induced by storms dissipate wave energy in shallow waters, which can significantly enhance the process of sediment resuspension, thereby affecting sedimentation dynamics. Ma, *et al.* [2] found that alongshore currents play a crucial role in coastal morphology change during a storm. Xia, *et al.* [11] found that typhoons that make landfall on the south side of the Yangtze River Estuary experience greater storm surge than those that make landfall on the front and north sides. When the typhoon storm surge, upstream flood peak, and astronomical spring tide are combined, the storm surge will be more significant. Similarly, according to the study by Pan and Liu [8], extreme storm surges may induce coastal inundation in Yangtze Estuary regions and relative sea level rise could reach 0.7m in the worst-case scenario.

Jiangsu Province is located on the eastern coast of China, which is often affected by active tropical cyclones in the northwest Pacific. According to Zhang, *et al.* [9], there are an average of three typhoons affecting Jiangsu Province annually. Typhoons that threaten Jiangsu Coast (JC) can be divided into three types: typhoons that move northward after landfall in Zhejiang or Fujian, typhoons that directly land along the coast of Jiangsu, and typhoons that operate in the coastal areas. These types of typhoons have a significant impact on the hydrodynamics and sedimentary dynamics of the JC. However, the adverse weather and oceanic conditions experienced during typhoons have posed significant obstacles to the direct observation efforts [10,12,13]. There is still a lack of in-depth research on the impact of different TC tracks and intensities with various tidal conditions on the sedimentary dynamics processes in JC due to the scarcity of observational data collected during TC events.

In this study, we developed a wave-current-sediment coupled model in JC and explored the hydrodynamics, sediment transport and morphological change during typhoon events. The main objectives were: (1) to investigate the response of hydrodynamics and sediment dynamics to TC, (2) to compare the effect that different tracks and intensities of typhoons have on hydrodynamics and sediment dynamics, and (3) to examine the tidal effects on sedimentary dynamics during TC events in JC. To achieve these objectives, we adopted the Finite Volume Community Ocean Model (FVCOM) and SWAN model as the ocean model and wave model, respectively. Subsequently, a total of eleven sets of experiments were designed based on different typhoon tracks, intensities, and tidal conditions.

2. Regional setting and study domain

Jiangsu Coast (JC) is located on the west coast of the South Yellow Sea and it is an important eastern coastal area in China. The coastline starts from the Xiuzhen River mouth at the border of Jiangsu and Shandong in the north and ends at the northern mouth of the Yangtze River in the south. The mainland coastline of JC is 734.84km long, and the length of the island coastline is about 84.74km. This study took the entire coastal area of Jiangsu Province as the study domain, with a latitude and longitude range of 31.5 °~35.1 ° N and 119 °~123 ° E [14].

The offshore shoals cover a vast area in JC, with a total area of 5000 km² of uncultivated coastal mudflat. According to sediment distribution characteristics, JC can be roughly divided into four sections from north to south: the northern part is the sandy, bedrock, and muddy coast of Haizhou Bay, the central part is the eroded coast of the abandoned Yellow River Delta, the central southern part is the radial sand ridge area, and the southern part is the coast of the Yangtze River Delta [14]. In general, Except for the north, the coastline is mainly muddy. Between 1128 and 1855, the ancient Yellow River

carried a large amount of sediment into the Yellow Sea, causing sedimentation and the significant eastward expansion of JC. After the Yellow River returned back to the Yellow Sea in 1855, the coastal dynamic conditions had been changed [15]. After erosion, transportation, and sedimentation of sediment dynamic process, the typical muddy nearshore area in China was shaped. The RSR system in the South Yellow Sea is a unique landform that extends from the Yangtze River Delta to the Sheyang River north of Jianggang, spanning 200 kilometers and 90 kilometers in length. Over 70 sand ridges extend from Jianggang offshore to the Yellow Sea, which is considered one of the most spectacular coastal landscapes in the world [1,16,17].

JC is located in a transitional monsoon climate region between the northern subtropical and warm temperate zones and is influenced by both oceanic and continental climates. The climate is distinct in four seasons, cold in winter and hot in summer, with an annual mean temperature of 13-16℃and an average annual precipitation of 804-1150mm, mainly concentrated from June to September. The annual mean wind speed in Jiangsu offshore is relatively high, reaching 6-10m/s. In winter, the prevailing wind direction is northeasterly, while in summer, it shifts to southeasterly. The frequency of occurrence of significant wave heights greater than 2m in Jiangsu offshore is relatively small, with the highest significant wave heights in Rudong outer sea and Haizhou Bay, while the lowest in the abandoned Yellow River estuary. JC is susceptible to tropical cyclones in summer, and the time affected by typhoons is between May and October, peaking in August and September. From 2000 to 2008, the southern region of JC experienced an average of 1.86 typhoons per year, while the northern part was impacted by an average of 0.72 typhoons annually.

Typhoon Lekima was a typical strong TC that affected JC in China. It formed in the northwest Pacific on August 4, 2019, made landfall in Zhejiang Province on August 10 with maximum wind speeds (Vmax) reaching 52 m/s, then moved towards Jiangsu Province with reduced wind speed (Vmax=23m/s). The typhoon eventually dissipated over the Bohai Sea on August 13, 2019. Its passage resulted in significant economic losses exceeding 74 billion dollars in mainland China [1,18,19]. This study takes No.1909 Typhoon Lekima as an example to investigate the dynamic processes in JC under the impact of TCs.

3. Materials and methods

3.1. Data collection

In order to calibrate the model parameters, we collected validation data during the passage of No.1909 Typhoon Lekima from July to August 2019. The water level and current validation data of this study were obtained from the National Marine Data Center (https://mds.nmdis.org.cn/). The measured wave validation data and other model wave validation data were obtained from Yang, Li, Zhong, Pan, Zhao and Dong [1] and the storm surge-wave analysis dataset [20], respectively. Due to the lack of field sediment observation data, the model was calibrated using remote sensing (GOCI) data (https://kosc.kiost.ac.kr/). Besides, hourly sea surface wind forcing data was downloaded from the fifth generation ECMWF atmospheric reanalysis of the global climate (ERA5) (https://cds.climate.copernicus.eu) for capturing the dynamic process during typhoons' passage.

3.2. Numerical model

FVCOM [21] is a three-dimensional hydrodynamic model that uses an unstructured mesh and a σ-stretched coordinate system. The model was applied in this study to simulate hydrodynamics and sediment dynamics in JC during TCs' passages. The model was configured as the modified Mellor and Yamada level 2.5 (MY-2.5) [22] for vertical mixing and Smagorinsky [23] turbulent closure scheme for horizontal mixing. It is adept for the complex coastlines of coastal areas[24-27]. The SWAN model, developed by Booij, *et al.* [28], was employed to simulate wind-wave generation and propagation processes. In addition, the sediment module used in this study is FVCOM-SED, which has been

extensively applied in coastal areas [18,29-31]. The wave model SWAN was run separately and input the wave field into FVCOM, which is called one-way wave-current coupling.

3.3. GOCI satellite remote sensing suspended sediment concentration (SSC) retrieved algorithm

GOCI (Geostationary Ocean Color Imager) is a sensor mounted on the first geostationary orbit ocean color satellite of the world, COMS (Communication, Ocean and Meteorological Satellite), launched by South Korea. The central longitude and latitude of the GOCI image is 130 ° E and 36 ° N, respectively. The coverage area is 2500 km x 2500 km, and the spatial resolution is 500 m. GOCI has a time resolution of 8 scenes per day and 1 scene per hour, with imaging times ranging from 00 hours to 07 hours in world time. Based on its high temporal resolution, GOCI data has been widely used in the study of SSC distribution and transport in nearshore areas [32].

We selected cloud-free images of the JC area, captured on July 20 and August 2, 2019, to verify the modeled surface SSC. The study used the retrieved algorithm for sea surface SSC by He, *et al.* [33], which is widely used in high SSC areas such as Hangzhou Bay [26,32]. It is speculated that this method is also applicable to the JC area. The surface SSC values retrieved algorithm is as follows:

$$SSC = 10^{1.0758+1.1230\times\frac{ref(745nm)}{ref(490nm)}} \quad (1)$$

where SSC indicate the suspended sediment concentration (unit: mg/L), $ref(745\,nm)$ and $ref(490\,nm)$ are the remote sensing reflectance of the 745 and 490 nm bands of the GOCI satellite, respectively.

3.4. Model configuration

3.4.1. Model setup and initial conditions

The model domain is depicted in Fig. 1. In this study, we employed the Surface-water Modelling System (SMS) to create grids based on the 2022 Google Earth coastline data. The bathymetry data in the JC area were obtained from the 2019 electronic chart, while bathymetry data for the remaining area in the model domain was obtained from the ETOPO1 Global Relief Model. The grid resolution within the JC ranges from 100 m to 300m nearshore, while the opening boundary is 10 km. The model employed a uniformed sigma-stretched coordinate system consisting of six vertical layers. In order to drive the hydrodynamic model along the open boundary, the NAO.99b short-period Ocean tide model was utilized, considering 16 major constituents (M2, S2, K1, O1, N2, P1, K2, Q1, M1, J1, OO1, 2N2, Mu2, Nu2, L2, T2) [34]. Furthermore, identical grids and wind were applied in the SWAN model to simulate the wave propagation within the model domain. The wave spectrum was calculated in the 0.031-0.548 Hz range and divided into 40 frequency steps according to the logarithmic distribution. The rest of the parameters were given the default settings in the SWAN manual.

According to the General Report on Comprehensive Survey and Evaluation of Offshore Oceans in Jiangsu Province [14], there are significant differences in the zoning of sediment in JC. The median particle size distribution of sediment in Haizhou Bay, Abandoned Yellow River Estuary, Radial Sand Ridge, and Yangtze River Estuary ranges from 0.01 to 0.08mm. Therefore, the setting of sediment parameters in the model has spatial heterogeneity. Based on the relationship between suspended sand particle size and sedimentation velocity measured experimentally, the settling velocity was set to 0.3~3.8 mm/s [35]. According to the empirical formula of particle size and erosion rate, the erosion rate was set to 2×10^{-5}~5×10^{-5} kg/m^2/s. The critical erosion stress was set to be 0.6~0.12 N/m^2, while the critical deposition stress was set at a constant value of 0.05 N/m^2.

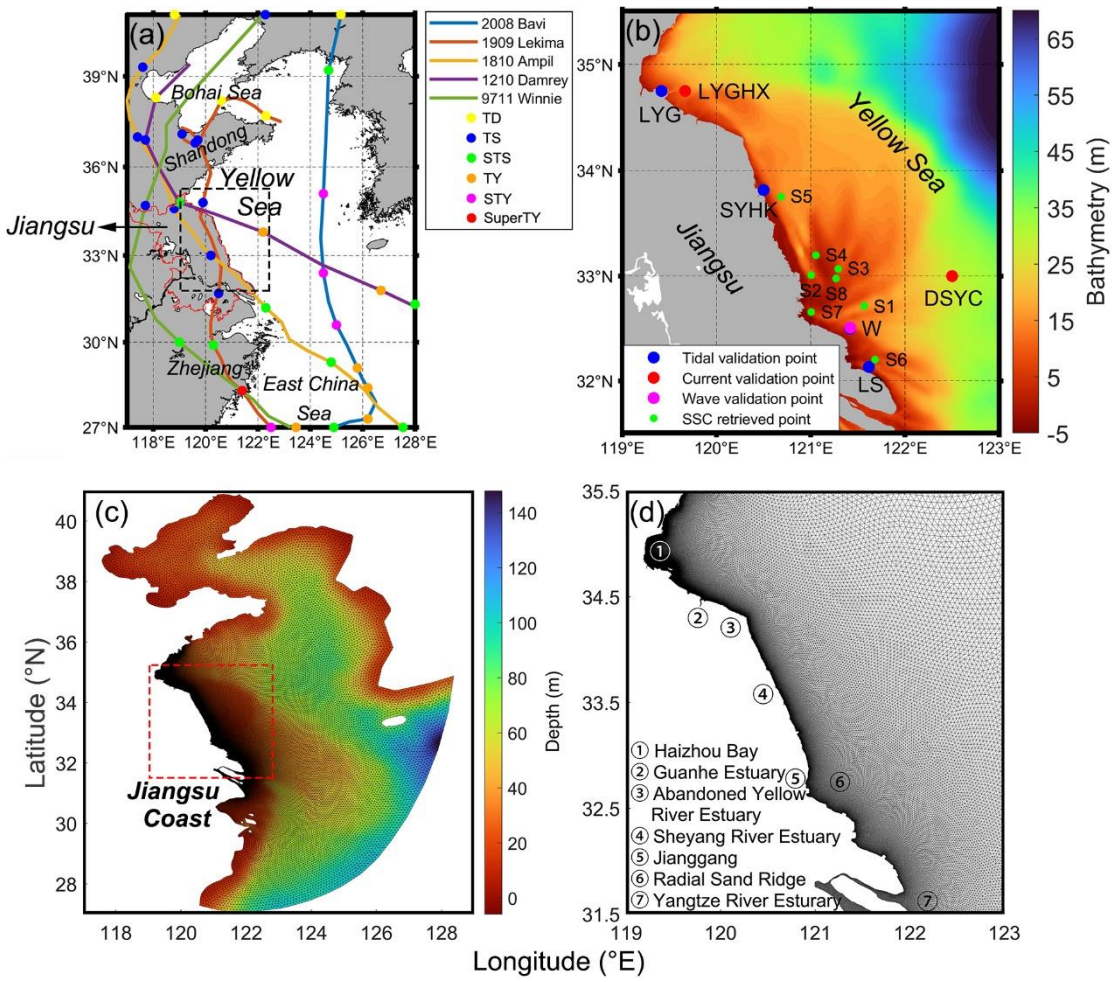


Figure 1. (a) Typical typhoon tracks and intensity diagram influencing JC. The polygonal area enclosed by the red line is the scope of Jiangsu Province. The area surrounded by a black dashed rectangle is the scope of JC. (b) The bathymetry of JC and the verification points distributed within the region. (c) Grids and bathymetry of the model domain. The region represented by the red dashed box is JC. (d) The grids within the JC region. The numerical number represents the corresponding place name.

Table 1. Main parameters used in the coupled model.

Model parameters	Value
Number of mesh nodes and elements	92068, 178933
Model external time step	1.0 s
Model internal time step	10 s
Median grain size	0.01-0.08 mm
Settling velocity	0.3-3.8 mm/s
Critical erosion stress	0.6-0.12 N/m^2
Critical deposition stress	0.05 N/m^2
Erosion rate	2×10-5-5×10-5 kg/m^2/s
Porosity	0.5

3.4.2. Numerical experiments setting

A total of 11 experiments were designed to explore different factors, such as typhoon tracks, intensities, and tidal superposition conditions to the impact of hydrodynamics and

sedimentary processes in JC. The track of No.1909 Typhoon Lekima represents a typical example of passing through JC after making landfall in the south of JC; The track of No.1210 Typhoon Damrey is a representative of landfall along the northern coast of JC; No. 1810 Typhoon Ampil's track is a typical path of landfall along the southern JC; No.2008 Typhoon Bavi passed through the Yellow Sea and affect JC, which is a typical representative of this type of typhoon. Among them, experiments 1-4 are under the influence of four typical typhoons, with tides and waves taken into account; Experiments 5-8 show the situations when the wind forcing of four typical typhoons is amplified by 1.3 times; Experiment 9 selected No.9711 Typhoon, which had a significant impact in JC; Experiment 10 excluded the tidal effects and only considered the effects of wind forcing and waves from Lekima on hydrodynamics and sedimentary dynamics; Experiment 11 assumes that Typhoon Lekima occurred during the astronomical spring tide period. All experiments were preheated for 10 days before starting, without considering the effects of runoff, temperature, and salinity. The detailed configuration description of the experiment is shown in Table 2.

Table 2. Experiments description.

Experiment	Description
Exp.1	Forced by wind, tidal current, and waves during the No.1909 Typhoon Lekima
Exp.2	Same with Exp.1, but during the No.2008 Typhoon Bavi
Exp.3	Same with Exp.1, but during the No.1810 Typhoon Ampil
Exp.4	Same with Exp.1, but during the No.1210 Typhoon Damrey
Exp.5	Same with Exp.1, but the wind force was amplified 1.3 times
Exp.6	Same with Exp.2, but the wind force was amplified 1.3 times
Exp.7	Same with Exp.3, but the wind force was amplified 1.3 times
Exp.8	Same with Exp.4, but the wind force was amplified 1.3 times
Exp.9	Same with Exp.1, but during the No.9711 Typhoon
Exp.10	Same with Exp.1, but without the tidal effect
Exp.11	Same with Exp.1, but during the spring tide cycle

3.4.3. Model validation

As was shown in Fig. 2a-h, the observed and modeled tidal elevation, tidal currents, and waves were compared to calibrate the model. The water elevation data was collected from July 25 to August 24 (2019) at LS (Lvsi), SYHK (Sheyang River Estuary) and LYG (Lianyungang). The tidal currents data were measured at stations DSYC and LYGHX during the neap tide from 00:00 on July 26 to 27, 2019, and during the spring tide from 00:00 on August 3 to 4, 2019. The wave data was collected from 22:00 on August 6 to 2:00 on 13 August 2019 at station W. In addition, we obtain a wave reanalysis dataset during storm events in the Yellow Sea for significant wave height verification.

The sediment module was calibrated using remote sensing (GOCI) data. Eight cloud-free images captured from 00:00 to 07:00 (UTC) on 2 August 2019 were selected to verify the magnitudes and trends of the modeled surface SSC at the 8 stations (S1-S8), which was shown in Fig. 2i-p. Besides, the retrieved surface SSC field in JC at 04:00 on July 20th (UTC) and 04:00 on August 2nd (UTC) was validated with the modeled SSC (Fig. 3a-d).

To verify the accuracy of the coupled model for hydrodynamic and sediment dynamics, root mean square error (RMSE) and correlation coefficient (CC)[36] for tidal elevation, tidal currents, waves, and SSC were calculated as shown in Table 3. The formula for statistics is as follows:

$$RMSE = \sqrt{\frac{1}{n}\sum_{i=1}^{n}(m_i - o_i)^2} \quad (2)$$

$$CC = \frac{1}{n}\sum_{i=1}^{n}\frac{(m_i - \bar{m})(o_i - \bar{o})}{S_m S_o} \quad (3)$$

where m_i and o_i represent the modeled and observed values at time t, which have mean values $\bar{m}$ and $\bar{o}$, and standard deviations S_m and S_o, respectively. The smaller the RMSE, the smaller the deviation between the modeled and observed values. A value of CC close to 1 suggests a strong agreement between the observed and model values.

The error statistics of the model results (Table 3) show a strong correlation with the observed water level and significant wave height values, with CC higher than 0.89. The CC of current magnitude and direction performance correlation is categorized as moderate (0.4-0.6), with RMSE lower than 0.26m/s. The CC value of SSC near the surface level is relatively lower, but the RMSE is within an acceptable range (20-165mg/L). In addition, the modeled surface SSC distribution pattern was consistent with the GOCI data for the area of JC. As a result, the coupled model demonstrates satisfying performance in accurately simulating regional ocean dynamics and sediment transport.

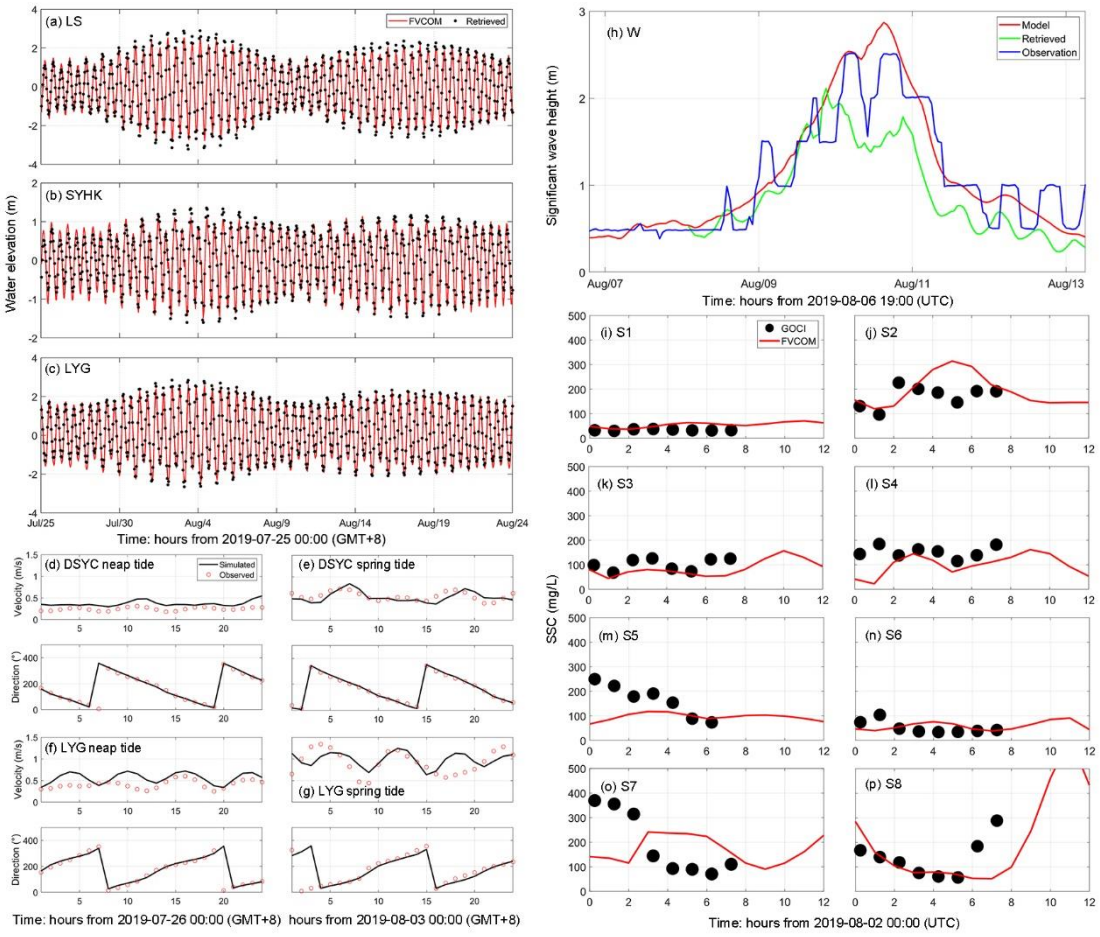


Figure 2. From July 25th to August 24th, 2019, hourly water level validation at three tidal stations: LS (Lvsi) (a), SYHK (Sheyang River Estuary) (b), and LYG (Lianyungang) (c); Verification of current at DSYC and LYG during spring and neap tides respectively (d-g); At site W, the validation between the simulated significant wave height (red line) of SWAN, the obtained wave reanalysis dataset (green line), and the measured values (blue line) (h); Hourly after 0:00 (UTC) on August 2, 2019, at

the S1-S8 SSC verification point, the comparison (i-p) between the GOCI retrieved and the simulated SSC.

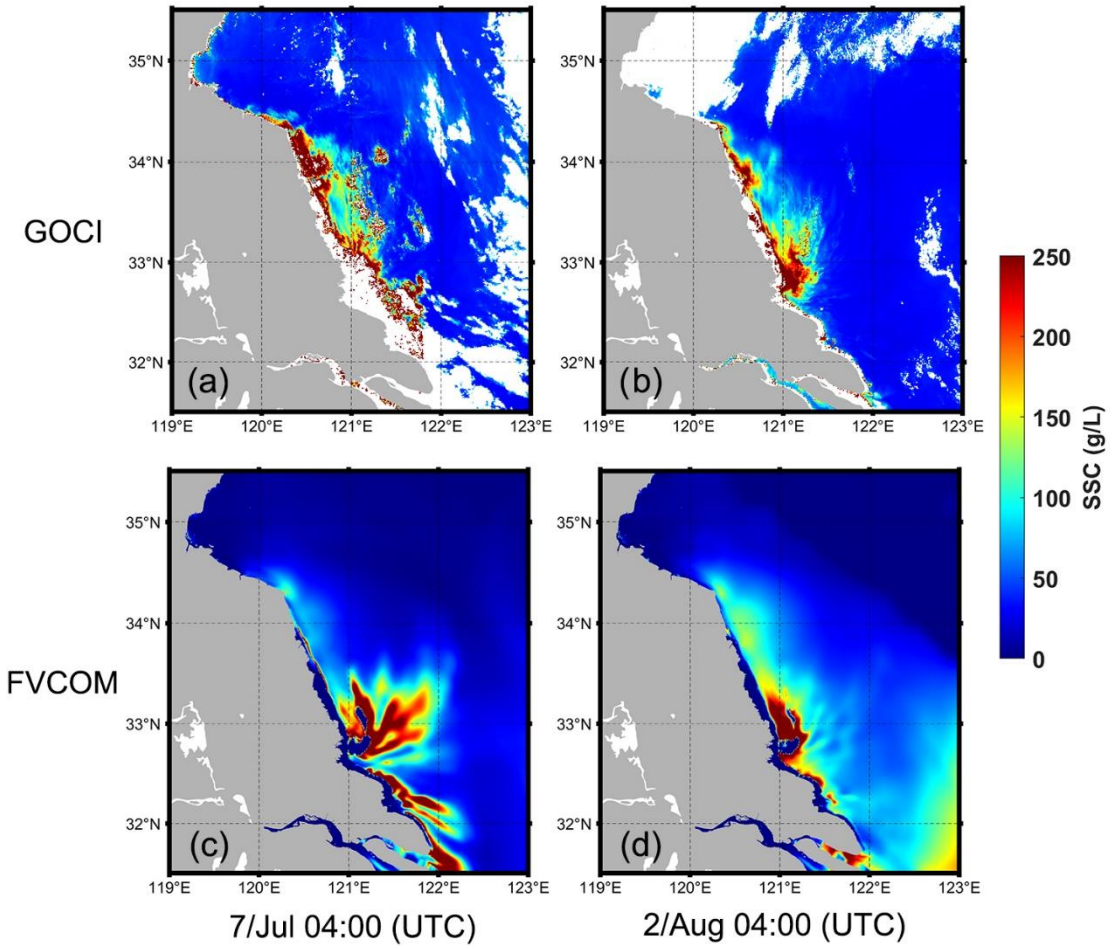


Figure 3. Distribution of sea-surface SSC in JC obtained from GOCI retrieved (a-b) and FVCOM modeled (c-d) at 04:00 (UTC) on July 20 and 04:00 (UTC) on August 2, 2019, respectively.

Table 3. Error statistics of the model results.

Types	Items	CC	RMSE
Water level	LS	0.97	0.37m
	SYHK	0.95	0.21m
	LYG	0.97	0.33m
Current velocity	DSYC neap tide	0.60	0.13m/s
	DSYP spring tide	0.55	0.10m/s
	LYG neap tide	0.54	0.18m/s
	LYG spring tide	0.39	0.26m/s
Significant wave height	W	0.89	0.33m
Sea-surface SSC	S1	-0.23	19.85mg/L
	S2	0.18	85.13mg/L
	S3	0.17	43.34mg/L
	S4	-0.02	77.37mg/L
	S5	-0.21	162.10mg/L

	S6	-0.52	32.98mg/L
	S7	-0.75	165.31mg/L
	S8	0.03	104.84mg/L

4. Results

4.1. The response of hydrodynamics and sedimentary dynamics to Typhoon Lekima

Fig. 4 shows the differences between hydrodynamics and sedimentary dynamics under fair weather conditions and Typhoon Lekima. The right column graph represents the time when Typhoon Lekima significantly impacted JC (2019-08-10 23:00 UTC). To eliminate the tidal effects on currents and SSC, the similar tidal period that occurred 14 days ago when the wind speed was relatively low (2019-07-26 22:00 UTC) was selected as the fair weather conditions.

Under fair weather conditions, the sea surface wind speed was relatively small, generally within 5m/s, with the significant wave height (Hs) around 0.5m. At the moment significantly affected by the typhoon, the center of the TC was located on the land of Jiangsu Province, with the direction of the wind field rotated counterclockwise. The lower friction force on the sea surface allowed for higher southeasterly wind speeds, reaching over 20m/s. Correspondingly, the Hs also significantly increased compared to fair weather conditions, reaching over 5m in the outer sea area of JC. The Hs gradually decreased towards the nearshore, with smaller waves in the RSRs, but they can still reach about 1m (Fig. 4a1-a2).

At this moment under fair weather conditions, the direction of the surface and bottom currents was basically the same, with the tidal currents converging centripetally in the RSRs. Here, the SSC was slightly higher, but generally less than 0.25g/L. However, during the typhoon, the flow field was very different compared to fair weather conditions at a similar tidal period. The strong southerly wind caused by the typhoon enhanced the southeast direction currents on the south side of the RSRs, with a current velocity of over 1m/s. In areas with higher wind speeds in JC, the effect on the surface currents was more significant. Correspondingly, there was a significant increase in surface SSC compared to fair weather conditions, and there was a high-value area of SSC in the entire Jiangsu coastal area, which could reach 1.5-2g/L on the southern side of the RSRs. On the north side of the RSRs, the bottom layer flow velocity differed significantly from fair weather conditions, shifting from northwest to southeast direction. The SSC in the bottom layer was higher than that in the surface layer, generally between 1-2g/L, and could reach over 3g/L in the area from the abandoned Yellow River Estuary to the Sheyang River Estuary where the wave height decreased rapidly. The strong wave energy dissipation in shallow water greatly increases the shear stress on the seabed, enhances the process of sediment resuspension, and thus significantly increases the SSC (Fig. 4b1-b2 and c1-c2).

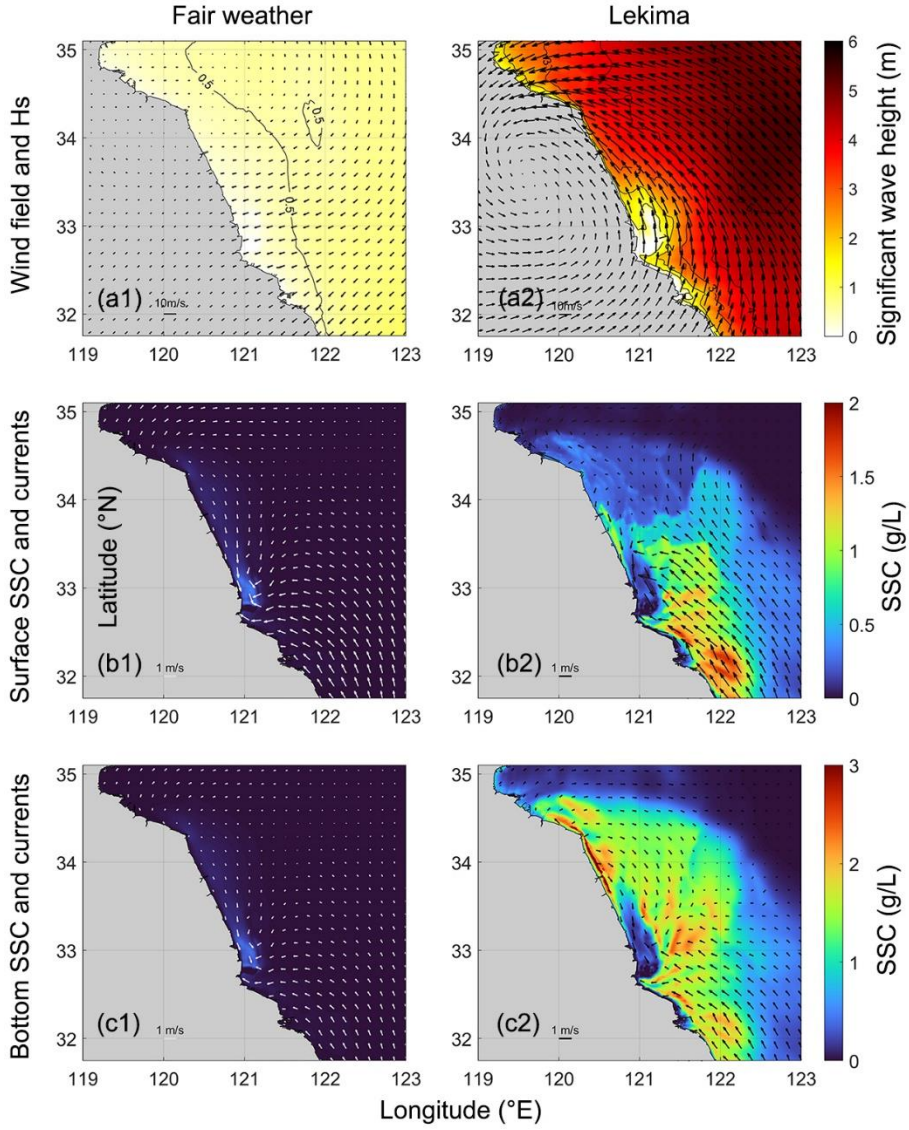


Figure 4. The significant wave height and wind field (a1-a2), surface currents with SSC (b1-b2), and bottom currents with SSC (c1-c2) at the similar tidal period during the passage of Typhoon Lekima (23:00 10 August) and under fair weather conditions (22:00 26 July).

Fig. 5 shows a tidal cycle before and after the passage of Typhoon Lekima, the wind, current, significant wave height, bottom stress, water level, SSC, and their vertical time series distribution located at point W near the RSR area. During the typhoon period, the wind speed significantly increased, reaching about 20m/s, with a southeast wind direction. The prevailing wind direction before the typhoon passed was mainly southerly, and it shifted to northerly after the passage. During the period of typhoon impact, the sea currents, originally dominated by tidal effects, underwent significant changes, with a noticeable increase in current velocity. At the peak flow velocity, the currents flowed from southwest to northeast. During the passage of the typhoon, the significant wave height reached 4 meters, whereas, under fair weather conditions, it generally did not exceed 1 meter. Correspondingly, during the typhoon's passage, both bottom stress and SSC exhibited noticeable increases. Originally, SSC and bed shear stress were significantly correlated with tidal cycles. However, Typhoon Lekima occurred during a period of neap tides, during which the relatively small bottom stress increased significantly. The sustained high bottom stress resulted in a significant increase in SSC, with the SSC in the bottom layer being greater than that in the surface layer. The depth-averaged SSC could reach 1 g/L during the typhoon's passage, nearly a hundredfold increase compared to SSC levels during neap tides

under fair weather conditions. The peak SSC occurred during the flood tide, which was related to the combined effect of a large wave current combined bottom stress at that moment. Following the passage of the typhoon, both SSC bottom shear stress rapidly returned to normal levels. Furthermore, during the impact of Lekima, there was a sequence of stormwater level decrease then followed by an increase, with the water level rise slightly exceeding the decrease, reaching around 0.5 meters. In situations of low wind speeds, the influence of wind forcing on water levels could be almost negligible.

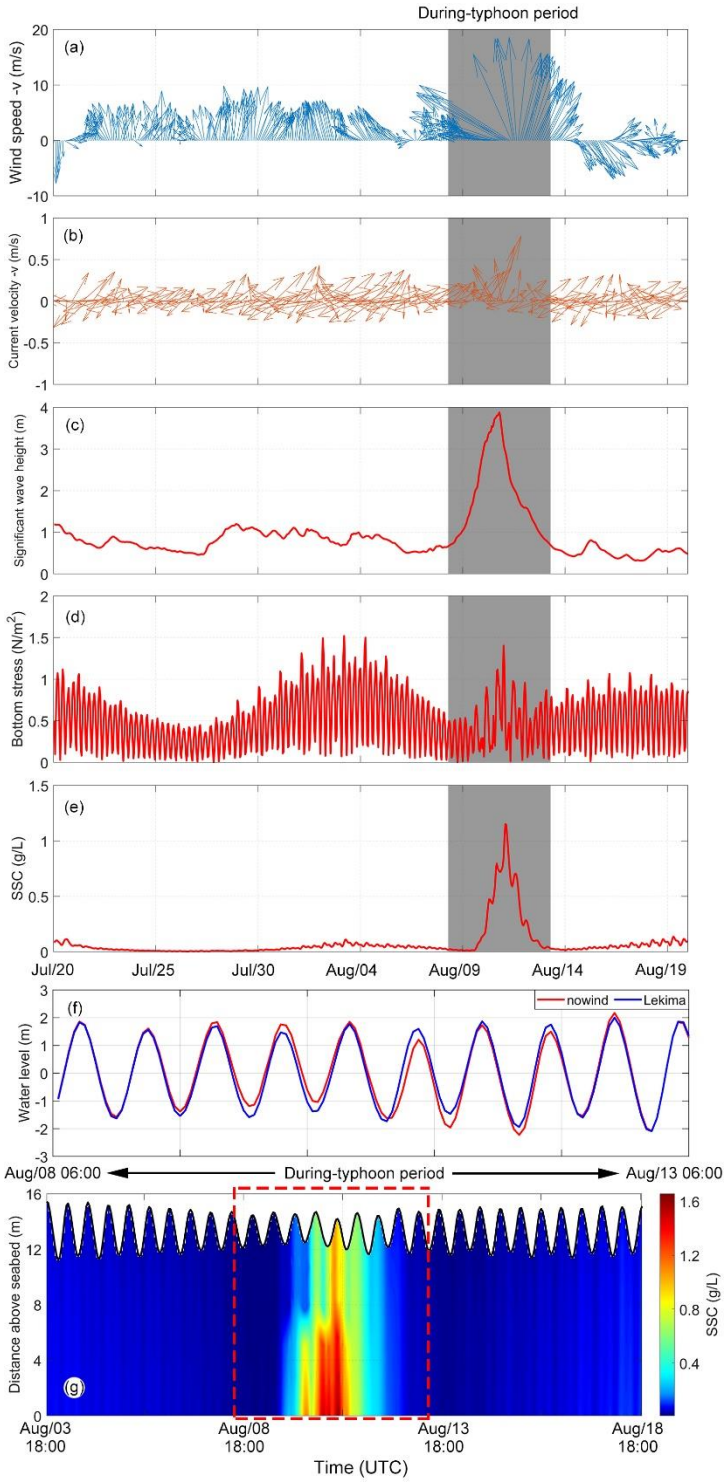


Figure 5. During a tidal cycle before and after the passage of Typhoon Lekima, (a) wind speed in the direction of v, (b) current velocity in the direction of v, (c) significant wave height, (d) bottom

stress, (e) SSC, (f) comparisons of water level under no-wind conditions and Typhoon Lekima, (g) SSC vertical profile time series. The gray area and the red dashed box represent the period of typhoon transit impact.

4.2. The impact of TCs with different tracks and intensities on sedimentary dynamics

To explore the impact of TCs with different tracks and intensities on sedimentary dynamics in JC, we selected four representative tracks of typhoons that affect JC. During the passage of four typical typhoons, except for Typhoon Bavi, the sediment flux induced by the other three typhoons in JC was directed northwestward from the southeast along the coastline. This pattern was attributed to the prevailing easterly or southeasterly wind anomalies during these typhoon passages. However, as Bavi moved northward out of the Yellow Sea, with the JC nearshore located to its left, the prevailing wind anomalies were mainly northwesterly, and the magnitude of the wind anomalies was relatively small. Consequently, the sediment flux induced by Bavi was relatively minor, reaching a maximum of only 0.2 kg/m/s (Fig. 6d and Fig. 7d1).

The magnitudes and patterns of sediment flux induced by Typhoon Lekima and Typhoon Damrey were quite similar. Near LS and the RSRs exhibited high sediment flux values, reaching over 0.8 kg/m/s. However, compared to Damrey, the wind anomalies associated with Lekima were larger in the offshore areas, reaching a maximum of 7 m/s, and relatively smaller nearshore, generally less than 3 m/s, with a prevailing southeasterly direction. In contrast, the wind anomalies associated with Damrey ranged between 4-6 m/s, with easterly winds prevailing in the southern part of the nearshore area of JC and southeasterly winds prevailing in the northern part. The wind anomaly pattern of Damrey was similar to that of Ampil, but the magnitude was slightly smaller, ranging between 3-5 m/s. Correspondingly, the sediment flux induced by Ampil was of a smaller magnitude compared to that induced by Damrey and Lekima. Additionally, during the passage of Ampil, the high sediment flux values were distributed in the offshore areas of the RSR, with no high-value area near LS, and the overall magnitude of the sediment flux ranged between 0.1-0.5 kg/m/s (Fig. 6a-c and Fig. 7a1-c1).

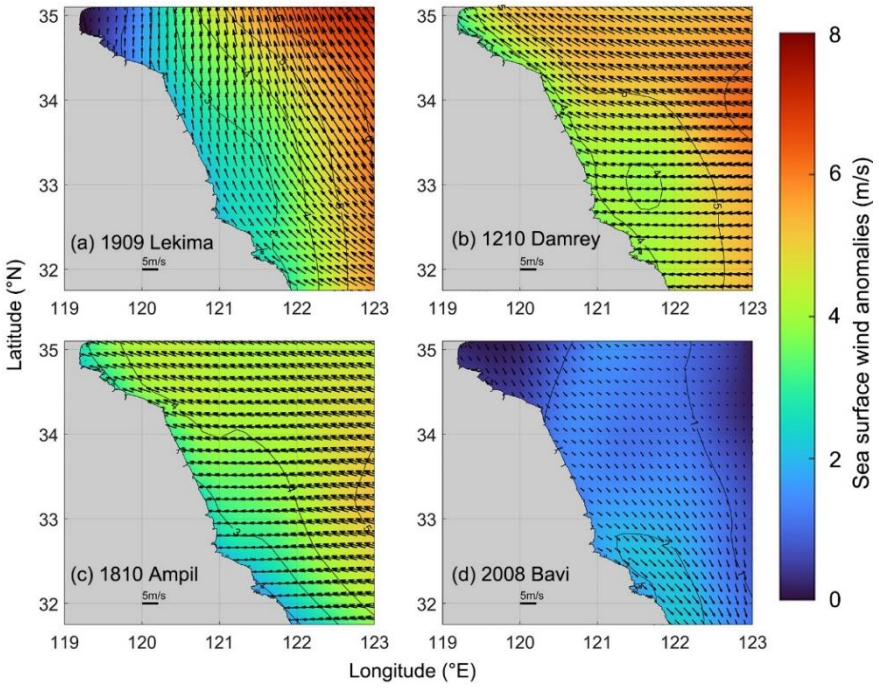


Figure 6. Typhoons (a) Lekima, (b) Damrey, (c) Ampil, and (d) Bavi induced wind anomalies in 5-day and the 30-year average (1991-2020) wind field in JC. The arrow represents the direction of the wind vector that deviates from the average wind field during the typhoon, and the color chart illustrates the wind anomaly.

After the passage of these four typhoons, model results indicated that there had been certain changes in the thickness of the seabed in JC. The most prominent feature was that the seabed exhibited a striped pattern with strong erosion/deposition closely related to the seafloor topography. Particularly in the RSRs, seabed erosion often occurred over the sand ridges where water depth is relatively shallow, while sediment accretion occurred in deep channels. This is due to the barrier effect of the sand ridges, where suspended sediment particles in the ocean water column in the RSRs are captured and accumulate in the deep channels; whereas within the sand ridges, the strong shear stress from the combined action of waves and tidal currents enhanced the sediment resuspension process, leading to seabed erosion. The morphological changes induced by Bavi were minimal, with variations generally within 0.1m, which is closely related to the magnitude of sediment flux. On the other hand, the bed thickness changes caused by Damrey were most significant, with erosion/deposition in sand ridges and deep channels exceeding ±0.3m. The distribution pattern of seabed erosion/siltation caused by Ampil and Lekima was similar, but Ampil was slightly larger, with a maximum of around ±0.2m, while Lekima was within ±0.15m (Fig. 7a2-d2).

After the typhoon wind field was amplified by 1.3 times, the sediment flux in JC significantly increased, especially with Damrey and Ampil, large areas of high sediment flux exceeding 1kg/m/s appeared throughout the nearshore waters of JC. The direction of sediment flux remained largely unchanged. Compared to the original conditions, the increase in sediment flux caused by the strengthened wind field of Lekima was not significant, with only high-value areas of around 1kg/m/s appearing near LS. The impact of the strengthened wind field of Bavi on the sediment flux near the north side of the Yangtze River Estuary was significant, inducing sediment flux towards the south exceeding 0.75kg/m/s. Under the influence of the strengthened wind fields of Damrey and Ampil, a certain degree of sediment accretion occurred in the seabed of the Yellow Sea north of 33°N, while significant seabed erosion occurred in the south of 33°N. The distribution pattern of erosion and deposition in the RSRs remained largely unchanged, but there was a noticeable increase in seabed thickness changes, especially with Damrey where there were large areas of ±0.3m variation near sand ridges and deep channels. Ampil was slightly weaker but still had a significant impact on the seabed morphology. The strengthening of the wind fields by Lekima and Bavi also increased the change in seabed thickness, with the rate of change increasing by about 50% (Fig. 7e1-h1 and 7e2-h2).

The above results indicate that typhoons landing in or passing through Jiangsu often bring sediment flux from southeast to northwest along the coast in JC, and the sediment flux increases with the typhoon wind speed. Conversely, typhoons passing northward in the Yellow Sea offshore can cause sediment flux from north to south, with a weaker impact on sediment dynamics if the typhoon center is relatively far from land. In terms of changes in bed morphology, typhoons induce strong stripe erosion/deposition at sand ridges and deep channels, with the intensity of erosion and deposition closely related to typhoon intensity.

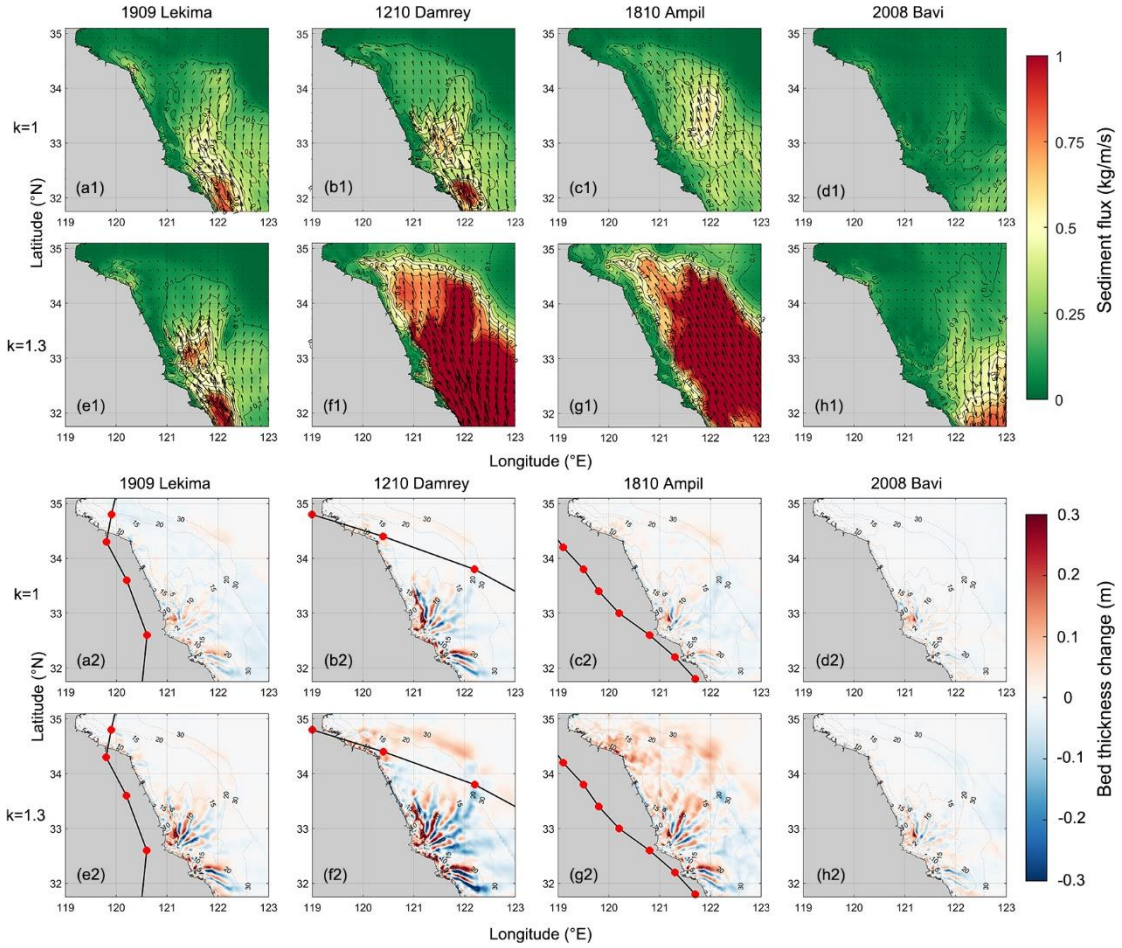


Figure 7. (a1-d1) represents the sediment flux in JC during a tidal cycle under the influence of Typhoon Lekima, Damrey, Ampil, and Bavi. The first-row k=1 represents the actual typhoon wind field, And the wind field in the second row (e1-h1) with k=1.3 corresponds to the wind field of the typhoon by 1.3 times. (a2-h2) represent the bed thickness changes under the influence of the corresponding typhoon and enhanced wind field, where the red dots and black lines represent the track of the corresponding typhoon, and the dashed lines represent the water depth.

5. Discussion

5.1. Example of TC affecting JC during the astronomical tidal period

No.9711 Typhoon Winnie, with strong winds and heavy rainfall, landed on the eastern coast of China on August 18, 1997. Coupled with astronomically high tides, a severe storm surge disaster occurred in the offshore areas of JC. Both Nantong Port and Lianyungang Port experienced record-breaking water levels. Significant coastal erosion and sedimentation, with extensive seawall damage, resulted in substantial economic losses [8,37].

The results shown in Fig. 8(I) indicate that in JC, the sediment flux caused by Typhoon 9711 was significantly higher than that of the four typical typhoons mentioned above. There existed a high-value area of sediment flux in the RSRs, reaching up to over 1.6 kg/m/s, with the direction along the coastline from southeast to northwest (Fig. 8(I)a). The distribution of sediment flux was closely related to the distribution of wind anomalies. The wind anomalies are also southeastward, decreasing in magnitude from southeast to northwest, ranging between 2m/s and 5m/s (Fig. 8(I)b). However, compared with other typhoons, the difference in wind anomalies was not significant, indicating that the large sediment flux was not solely caused by the intensity of the typhoon.

Regarding the morphological changes of the seabed, strong striped erosion and deposition patterns were exhibited at sand ridges and deep channels, with a maximum magnitude of approximately ±0.3m (Fig. 8(I)c). This finding closely aligns with the results of

Ya-zhen, *et al.* [38], who reported an average sediment deposition thickness of about 20cm in the southern port and northern passage of the Yangtze River estuary during Typhoon 9711. Furthermore, the geomorphological changes induced by Typhoon 9711 were significantly greater than those caused by the four typical typhoons, approaching the results of Typhoon Lekima with a 1.3-fold increase in wind field strength, and only slightly weaker than the results after Typhoon Damrey with a 1.3-fold increase in wind field strength.

5.2. Tidal conditions during different Typhoon impact periods

Fig. 8(II) illustrates the tidal conditions during different typhoon impact periods. The passage of Typhoons Lekima and Ampil were in the neap tide cycle, and the diurnal tidal range was relatively small. However, some fluctuations in tidal periodicity occurred, manifesting as storm surges and recessions. Typhoons Bavi and Damrey corresponded to periods between neap tide to spring tide and spring tide to neap tide, respectively, with tidal periodicity showing more regular and uniform changes. During the impact period of Typhoon 9711, it coincided with astronomical high tides, resulting in extreme storm surges and recessions. The maximum tidal ranges could exceed 5m (Fig. 8(II)a-e). Larger tidal ranges often lead to increased tidal current velocity, thereby increasing bed shear stress and promoting sediment resuspension processes, leading to a significant increase in SSC. The increased current velocity and SSC further intensified the sediment transport induced by the typhoon. This was a significant factor that the sedimentary dynamic process was affected by Typhoon 9711 more severely compared to other typhoons in JC.

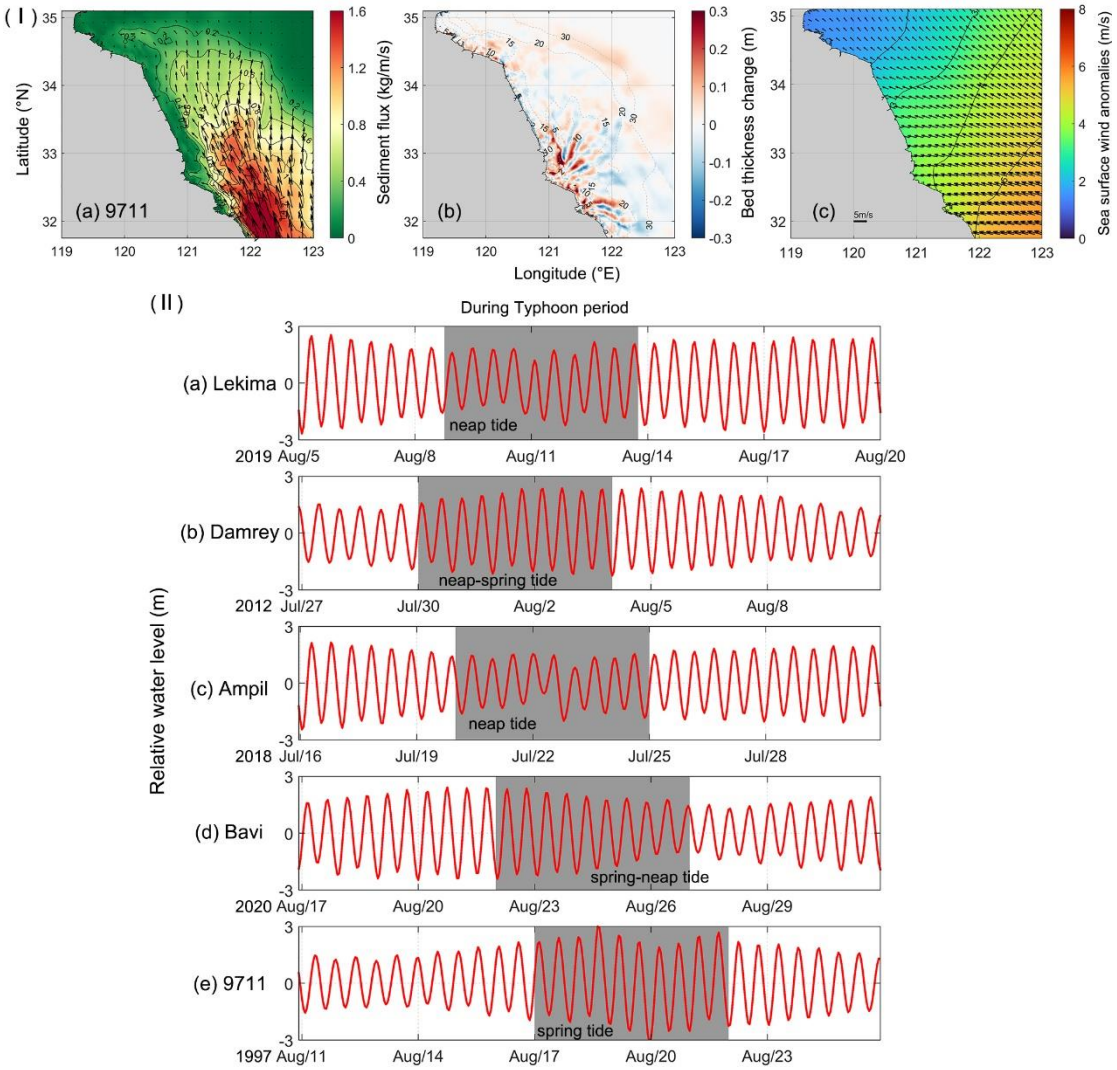


Figure 8. (I) During the tidal cycle of No.9711 Typhoon impact period, (a) sediment flux, (b) bed thickness change, and (c) sea surface wind anomalies over the 5 days affected by the typhoon. (II)Time series of Relative water levels during typical typhoons (a) Lekima, (b) Damrey, (c) Ampil, (d) Bavi, and (e) 9711 affected JC at point W.

5.3. The impact of different tidal conditions on sedimentary dynamics during typhoons

Fig. 9 indicates that if Typhoon Lekima occurs during spring tides, the sediment flux towards the northwest direction along the coast would significantly increase. In the RSRs, a high-value zone of sediment flux exceeding 1 kg/m/s was exhibited, approximately 80% to 100% higher than that during neap tides. If it was solely driven by wind forcing without tidal effects, the sediment flux was minimal, with a maximum of around 0.3 kg/m/s, predominantly directed towards the north, but significantly lower compared to neap tide conditions (Fig. 9a1-c1). Correspondingly, bed thickness changes in nearshore were closely associated with the magnitude of sediment flux. If there was no tidal forcing, the variations in bed thickness were minimal, with the maximum change around ±0.15m. In Exp.1 (during the neap tide), the extent of geomorphological changes was larger than in Exp.10 (without tidal influence), although the bed thickness changes were relatively smaller. However, in Exp.11 (during the spring tide), the bed thickness changes significantly increased, with the maximum change reaching up to ±0.3m, closely resembling the sediment flux and geomorphological changes induced by Typhoon 9711 (Fig. 9a2-c2).

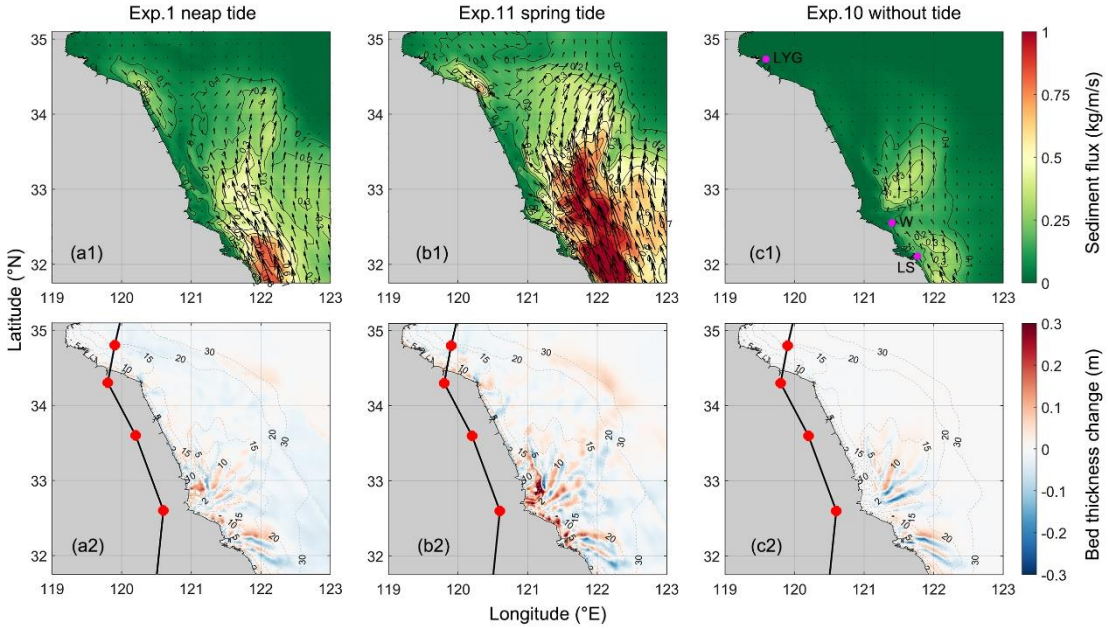


Figure 9. (a) During the neap tide period, (b) during the spring tide period, and (c) without tidal open boundary conditions, the sediment flux (row 1) and bed thickness changes (row 2) during the tidal cycle of Typhoon Lekima affecting JC.

Fig. 10 illustrates that at LS, LYG, and W points during both the spring and neap tide, SSC and bottom shear stress exhibited regular cyclic variations under tidal effect. At the moments of peak flood and peak ebb, both bottom stress and SSC were relatively high, while they were lower during high water and low water moments. Throughout the spring tide period, SSC and bottom stress at these points were notably higher compared to the neap tide period. A significant increase was exhibited at these points during the typhoon passage. Specifically, LS and LYG exhibited maximum bottom layer SSC ranging between 1.4-1.7 g/L and maximum bottom stress ranging between 1.5-2 N/m^2 during spring tide, while the SSC and bottom stress at point W, located in the RSR area, reached up to 4.5 g/L and 3 N/m^2, respectively. During neap tide, LS and W experienced maximum SSC at around 1 g/L and 2 g/L, approximately 40-60% of the levels exhibited during spring tide,

while the bottom stress was about 50-70% of that during spring tide. At LYG, the incremental changes in SSC and bottom stress between spring tide and neap tide were not significant, with SSC peaking at around 1.3 g/L and maximum bottom stress at approximately 1.2 N/m². Conversely, in the absence of tidal effects, the bottom shear stress was generally below 0.5 N/m², and post-typhoon passage, the bottom stress was negligible. Even during the typhoon passage, SSC levels were below 0.1 g/L, less than 10% of that during neap tide (Fig. 10a-f).

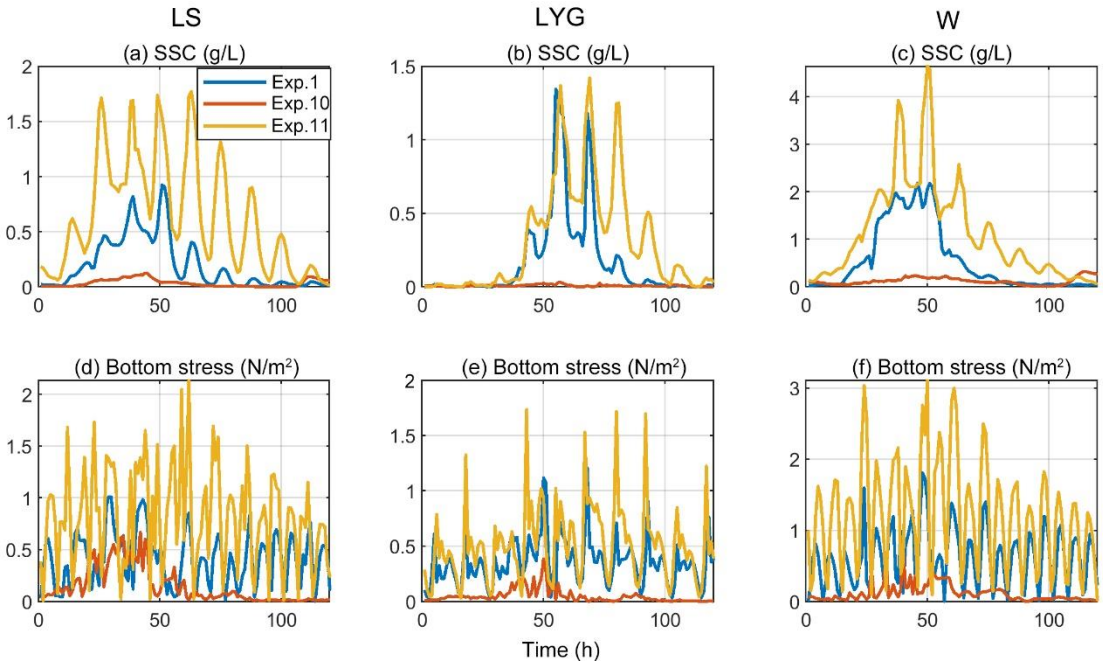


Figure 10. During the impact period of Typhoon Lekima, the time series of (a-c) bottom SSC and (d-f) bottom stress at LS, LYG, and W point under the conditions of Exp.1 (neap tide period), Exp.10 (without tide), and Exp.11 (spring tide period).

In summary, tidal effects play a fundamental and crucial role in the sediment net flux and geomorphological changes during typhoon passage. Under the combined influence of the typhoon and tidal effects, the increase in bottom shear stress leads to elevated SSC, resulting in a larger sediment flux. Particularly during spring tides, the net sediment flux induced by the typhoon can increase by 80%-100% compared to neap tides, accompanied by a significant rise in bed thickness changes. The findings are consistent with the conclusion of Fan, *et al.* [39], who found that coastal erosion is more severe during spring tides caused by a weak storm compared to neap tides caused by a strong storm.

6. Conclusion

Based on the FVCOM hydrodynamic model, SWAN wave model, and FVCOM-SED sediment module, this study constructed a 3D wave-current-sediment coupled numerical model for Jiangsu Coast (JC) to investigate the response of sediment dynamics to TCs under different scenarios. The main conclusions of the study are as follows:

(1) Typhoons ~~significantly and profoundly impact~~ the hydrodynamics and sediment dynamics of JC. During the passage of Typhoon Lekima (2019), under the influence of southeasterly winds exceeding 20m/s, current velocity, bottom stress, and significant wave height all increased significantly, with SSC reaching nearly a hundred times that of fair weather conditions.

(2) Comparative analysis of four different typical track typhoons showed that under the influence of typhoons following three typical tracks landing on the eastern coast of China, prevailing southeasterly winds brought a significant sediment flux from southeast

to northwest along the JC, with a large magnitude. The typhoon ~~which~~ did not land and moved northward in the Yellow Sea brought a relatively smaller sediment flux from north to south. Additionally, typhoons caused intense stripe-like erosion and deposition in the sand ridges and deep channels, with maximum seabed thickness variations of up to ±0.3m. The strengthening of typhoon wind fields led to more significant sediment flux and morphological changes in the seabed.

(3) During the impact of Typhoon 9711 within the spring tide cycle, its influence on sediment dynamics in JC is greater than that of other landfall typhoons. Through numerical simulation experiments, it was found that if Typhoon Lekima affects JC during spring tides, the net sediment flux within the tidal cycle can increase by 80% to 100% compared to the neap tide scenario, while in the absence of tidal effects, the net sediment flux caused by the typhoon is only 30-50% of that in the neap tide scenario. Furthermore, in the spring tide scenario, the impact of the typhoon on coastal geomorphological changes is significantly greater than under neap tide or no tide conditions.

This study demonstrates that not only the track and intensity of typhoons affect coastal sediment dynamics, but tidal effects play a fundamental and crucial role in this process, especially under spring tide conditions where tidal effects significantly amplify the impact of typhoons on sediment dynamics. While these findings are site-specific, the results of this study contribute to a better understanding of the tidal effects and differences of TCs under different scenarios, providing a theoretical basis for coastal management and disaster prevention and mitigation.

Author Contributions: Conceptualization, G.Y., C.L., C.Z. and J.Z.; Methodology, G.Y. and C.L.; Software, C.W., G.Y. and C.L.; Validation, C.W.; Formal Analysis, C.W.; Investigation, C.L.; Resources, X.M.; Data Curation, C.W.; Writing – Original Draft Preparation, C.W.; Writing – Review & Editing, J.Z. and C.Z.; Visualization, C.W.; Supervision, C.Z.; Project Administration, C.Z.; Funding Acquisition, C.Z.

Funding: This work was sponsored by the key project of the National Natural Science Foundation (42130405) and the Innovative and Entrepreneurial Talent Program of Jiangsu Province (R2020SC04).

Data Availability Statement: The data are available upon request.

Conflicts of Interest: The authors declare no conflicts of interest.

Appendix A

To strengthen the robustness of the model prediction performance, we collected field observation data in 2012 during Typhoon Damrey for model calibration. The results show that the simulation results are highly consistent with the observation results, which indicates that the coupled model has high credibility in predicting dynamic processes during TCs.

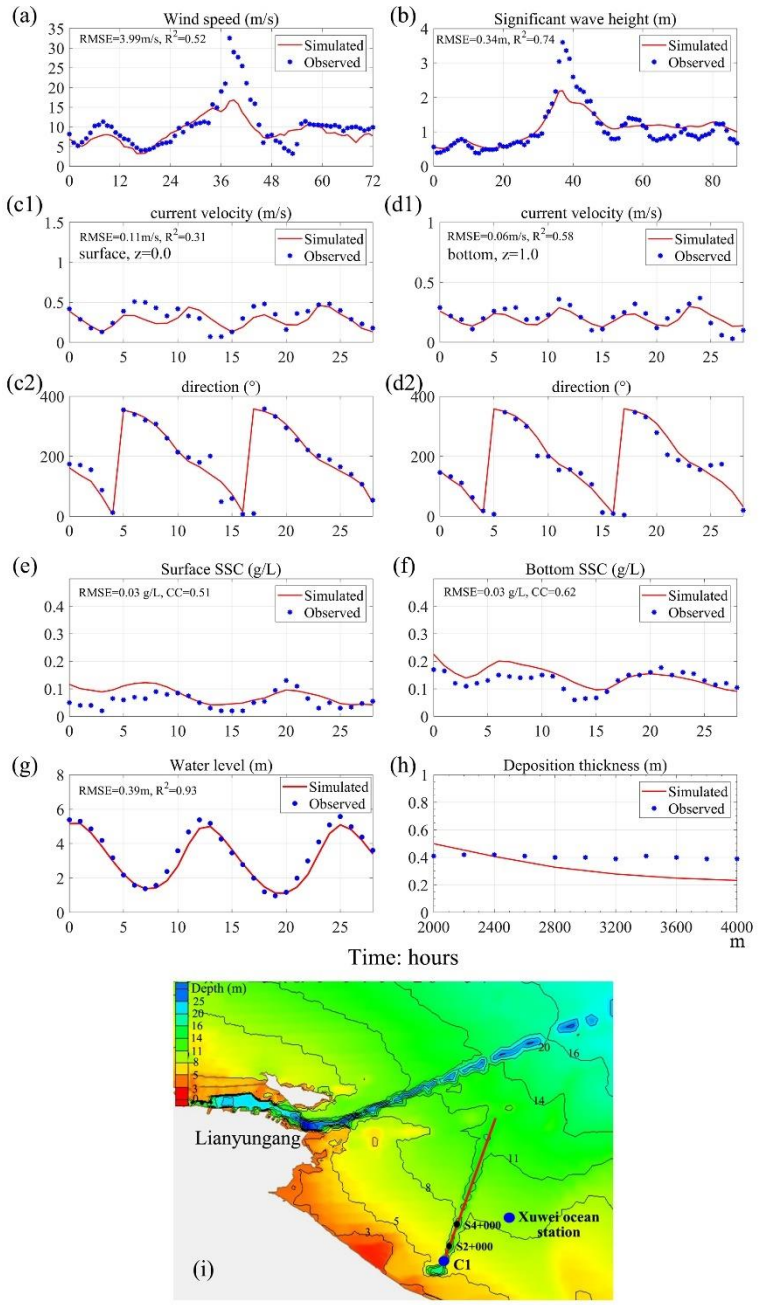


Figure A1. Comparisons between observed and simulated (a) wind speed and (b) significant wave height during Typhoon Damrey (2012) at Xuwei Ocean Station. Comparisons between observed and simulated (c1-d1) surface and bottom current velocity, (c2-d2) direction, (e-f) surface, and bottom SSC, and (g) water level at C1 point during August 2012. (h) Validation of deposition thickness at S2-S4 section in Xuwei approach channel after the passage of Typhoon Damrey. (i) Bathymetry map and the location of field stations.

References

1. Yang, G.; Li, C.; Zhong, Y.; Pan, X.; Zhao, C.; Dong, C. Impact of tropical cyclones on the hydrodynamics and sediment dynamics of the radial sand ridge system in the southern Yellow Sea. *Ocean Modelling* **2024**, *188*, 102328.
2. Ma, X.; Wang, C.; Zhao, C.; Ji, M.; Zhu, J.; Yang, G.; Li, C. Identification and simulation the response of storm-induced coastal erosion in the China Yellow sea. *Ocean Engineering* **2024**, *300*, 117394.
3. Trowbridge, J.; Nowell, A. Sediment transport events on shelves and slopes: STRESS. *(No Title)* **1994**.
4. Green, M.O.; Vincent, C.E.; McCave, I.N.; Dickson, R.R.; Rees, J.M.; Pearsons, N.D. Storm sediment transport: observations from the British North Sea shelf. *Continental Shelf Research* **1995**, *15*, 889-912.

5. Lu, J.; Jiang, J.; Li, A.; Ma, X. Impact of Typhoon Chan-hom on the marine environment and sediment dynamics on the inner shelf of the East China Sea: In-situ seafloor observations. *Marine Geology* **2018**, *406*, 72-83.
6. Emanuel, K. Increasing destructiveness of tropical cyclones over the past 30 years. *Nature* **2005**, *436*, 686-688.
7. Mei-e, R.; Ren-shun, Z.; Ju-hai, Y. Effect of typhoon no. 8114 on coastal morphology and sedimentation of Jiangsu Province, People's Republic of China. *Journal of Coastal Research* **1985**, 21-28.
8. Pan, Z.-h.; Liu, H. Extreme storm surge induced coastal inundation in Yangtze Estuary regions. *Journal of Hydrodynamics* **2019**, *31*, 1127-1138.
9. Zhang, M.; Zhou, C.; Zhang, J.; Zhang, X.; Tang, Z. Numerical simulation and analysis of storm surges under different extreme weather event and typhoon experiments in the South Yellow Sea. *Journal of Ocean University of China* **2022**, *21*, 1-14.
10. Cong, S.; Wu, X.; Ge, J.; Bi, N.; Li, Y.; Lu, J.; Wang, H. Impact of Typhoon Chan-hom on sediment dynamics and morphological changes on the East China Sea inner shelf. *Marine Geology* **2021**, *440*.
11. Xia, M.; Xu, F.; Wen, Y. Study of storm surge distribution along the Yangtze River and Estuary under different typhoon tracks. *The Ocean Engineering* **2022**, *40*, 115-122.
12. Ye, H.J.; Sui, Y.; Tang, D.L.; Afanasyev, Y.D. A subsurface chlorophyll a bloom induced by typhoon in the South China Sea. *Journal of Marine Systems* **2013**, *128*, 138-145.
13. Lapetina, A.; Sheng, Y.P. Simulating complex storm surge dynamics: Three-dimensionality, vegetation effect, and onshore sediment transport. *Journal of Geophysical Research: Oceans* **2015**, *120*, 7363-7380.
14. Office, J.P.S. *General Report on Comprehensive Survey and Evaluation of Offshore Oceans in Jiangsu Province*; Science Press: Beijing, 2012.
15. Wang, X.H.; Qiao, F.; Lu, J.; Gong, F. The turbidity maxima of the northern Jiangsu shoal-water in the Yellow Sea, China. *Estuarine, Coastal and Shelf Science* **2011**, *93*, 202-211.
16. Xing, F.; Wang, Y.P.; Wang, H.V. Tidal hydrodynamics and fine-grained sediment transport on the radial sand ridge system in the southern Yellow Sea. *Marine geology* **2012**, *291*, 192-210.
17. Xu, F.; Tao, J.; Zhou, Z.; Coco, G.; Zhang, C. Mechanisms underlying the regional morphological differences between the northern and southern radial sand ridges along the Jiangsu Coast, China. *Marine Geology* **2016**, *371*, 1-17.
18. Yu, Y.; Wang, Y.; Qiao, L.; Wang, N.; Li, G.; Tian, Z.; Zhong, Y. Geomorphological response of sandy beach to tropical cyclones with different characteristics. *Frontiers in Marine Science* **2022**, *9*, 1010523.
19. He, Y.; Chen, T.; Tang, J.; Chan, P.; Fu, J. Thermodynamic and Kinematic Structures in the Rainband Region of Typhoon Lekima (2019) at Landfall. *Atmosphere* **2022**, *13*, 312.
20. Zhang, J.; Xiong, M.; Zhang, W. Dataset for reanalysis of storm surges and waves during the cold wave process and typhoons in northern Jiangsu from 1987 to 2019. **2021**.
21. Chen; Liu, C.; Beardsley, H.; R., C. An unstructured, finite-volume, three-dimensional, primitive equation ocean model: application to coastal ocean and estuaries. 2003.
22. Mellor, G.L.; Yamada, T. Development of a turbulence closure model for geophysical fluid problems. *Reviews of Geophysics* **1982**, *20*, 851-875.
23. Smagorinsky, J. General circulation experiments with the primitive equations: I. The basic experiment. *Monthly weather review* **1963**, *91*, 99-164.
24. Wu, L.; Chen, C.; Guo, P.; Shi, M.; Qi, J.; Ge, J. A FVCOM-based unstructured grid wave, current, sediment transport model, I. Model description and validation. *Journal of Ocean University of China* **2011**, *10*, 1-8.
25. Yang, G.; Wang, X.H.; Zhong, Y.; Oliver, T.S.N. Modelling study on the sediment dynamics and the formation of the flood-tide delta near Cullendulla Beach in the Batemans Bay, Australia. *Marine Geology* **2022**, *452*.
26. Li, L.; Ren, Y.; Ye, T.; Wang, X.H.; Hu, J.; Xia, Y. Positive Feedback Between the Tidal Flat Variations and Sediment Dynamics: An Example Study in the Macro-Tidal Turbid Hangzhou Bay. *Journal of Geophysical Research: Oceans* **2023**, *128*, e2022JC019414.
27. Li, L.; Wang, X.H.; Andutta, F.; Williams, D. Effects of mangroves and tidal flats on suspended-sediment dynamics: Observational and numerical study of Darwin Harbour, Australia. *Journal of Geophysical Research: Oceans* **2014**, *119*, 5854-5873.
28. Booij, N.; Ris, R.C.; Holthuijsen, L.H. A third-generation wave model for coastal regions 1. Model description and validation. *Journal of Geophysical Research Atmospheres* **1999**, *104*, 7649-7666.
29. Yang, G.; Wang, X.H.; Zhong, Y.; Cheng, Z.; Andutta, F.P. Wave effects on sediment dynamics in a macro-tidal estuary: Darwin Harbour, Australia during the monsoon season. *Estuarine, Coastal and Shelf Science* **2020**, *244*, 106931.
30. Du, Y.; Cheng, Z.; You, Z. Morphological changes in a macro-tidal estuary during extreme flooding events. *Frontiers in Marine Science* **2023**, *9*, 1112494.
31. Ge, J.; Ding, P.; Chen, C.; Hu, S.; Fu, G.; Wu, L. An integrated East China Sea–Changjiang Estuary model system with aim at resolving multi-scale regional–shelf–estuarine dynamics. *Ocean Dynamics* **2013**, *63*, 881-900.
32. Wang, Z.; Qiao, L.; Gao, F.; Liu, Y.; Zhang, S.; Zhang, L. Sedimentary Dynamic Environment Changes Adjacent to the East China Sea Bridge. *Acta Sedimentologica Sinica* **2023**, 1-21.
33. He, X.; Bai, Y.; Pan, D.; Huang, N.; Dong, X.; Chen, J.; Chen, C.-T.A.; Cui, Q. Using geostationary satellite ocean color data to map the diurnal dynamics of suspended particulate matter in coastal waters. *Remote Sensing of Environment* **2013**, *133*, 225-239.
34. Ji, M.; Zhao, C.; Dou, X.; Wang, C.; Zhou, D.; Zhu, J. Identification and assessment of the drift velocity of green tides using the maximum cross-correlation method in the Yellow Sea. *Marine Pollution Bulletin* **2023**, *194*, 115420.

35. Kineke, G.; Sternberg, R. The effect of particle settling velocity on computed suspended sediment concentration profiles. *Marine Geology* **1989**, *90*, 159-174.
36. Murphy, A.H. Climatology, persistence, and their linear combination as standards of reference in skill scores. *Weather and forecasting* **1992**, *7*, 692-698.
37. Yin, B.; Xu, Z.; Huang, Y.; Lin, X. Simulating a typhoon storm surge in the East Sea of China using a coupled model. *Progress in Natural Science* **2009**, *19*, 65-71.
38. Ya-zhen, K.; Feng-yan, S.; Shou-xian, Z. A statistical model of storm-induced deposition in the north passage, Yangtze Estuary. *Journal of East China Normal University (Natural Science Edition)* **2003**, 80-86.
39. Fan, D.; Guo, Y.; Wang, P.; Shi, J.Z. Cross-shore variations in morphodynamic processes of an open-coast mudflat in the Changjiang Delta, China: With an emphasis on storm impacts. *Continental Shelf Research* **2006**, *26*, 517-538.

Disclaimer/Publisher's Note: The statements, opinions and data contained in all publications are solely those of the individual author(s) and contributor(s) and not of MDPI and/or the editor(s). MDPI and/or the editor(s) disclaim responsibility for any injury to people or property resulting from any ideas, methods, instructions or products referred to in the content.